FISIST/6-2000/CFIF
hep-ph/0005173

SNO and the neutrino magnetic moment solution of the solar neutrino problem

E. Kh. Akhmedov* and João Pulido†
Centro de Física das Interacções Fundamentais (CFIF)
Departamento de Física, Instituto Superior Técnico
Av. Rovisco Pais, P-1049-001 Lisboa, Portugal

Abstract

Assuming that the solar neutrino deficit observed in the Homestake, SAGE, Gallex, Kamiokande and Super-Kamiokande experiments is due to the interaction of the neutrino transition magnetic moment with the solar magnetic field, we calculate the expected values of a number of observables to be measured by SNO. For three model solar magnetic field profiles that produce the best fits of the previous data we calculate the charged current event rate, the (neutral current)/(charged current) event ratio and the charged current electron spectrum as well as its first and second moments. We study the dependence of the calculated observables on the choice of the magnetic field profile and on the value of the solar *hep* neutrino flux. We also compare our results with those obtained assuming that the solar neutrino problem is due to neutrino oscillations in vacuum or in matter. We show that there is an overlap or partial overlap between our predictions and those found for each of the oscillation solutions (SMA, LMA, LOW and VO). Given the uncertainties in the calculations and the expected uncertainties in the experimental results, the unambiguous discrimination between the two types of solutions to the solar neutrino problem (neutrino oscillations and magnetic moments) on the basis of the average rates and electron spectrum distortions appears to be difficult. The possible time dependence of the charged current signal and spectrum distortion in the case of the magnetic moment solution therefore remains the best hope for such a discrimination. For a hybrid solution (neutrino magnetic moment plus flavour mixing) the smoking gun signature would be an observation of $\bar{\nu}_e$'s from the sun.

*On leave from National Research Centre Kurchatov Institute, Moscow 123182, Russia. E-mail: akhmedov@cfif.ist.utl.pt
†E-mail: pulido@beta.ist.utl.pt

1 Introduction

The Sudbury Neutrino Observatory (SNO) [1] is capable of detecting solar neutrinos through charged current and neutral current neutrino deuteron reactions as well as through νe scattering. It is expected to perform precision measurements of a number of the characteristics of the solar neutrino flux. The forthcoming data from SNO will complement in a very important way the already available data of Homestake, SAGE, GALLEX, Kamiokande and Super-Kamiokande experiments [2], allowing crucial tests of the proposed solutions of the solar neutrino problem.

Recently, a comprehensive new study of the possible implications of the forthcoming SNO data for neutrino oscillation solutions of the solar neutrino problem has been performed by Bahcall, Krastev and Smirnov (hereafter BKS) [3, 4]. In the present paper we analyse possible implications of the SNO measurements for another particle physics solution of the solar neutrino problem which is currently consistent with all the data – the neutrino magnetic moment scenario. We also compare our predictions with those of BKS and discuss the possibilities of discriminating between the two scenarios.

Neutrinos with transition magnetic moments experience a simultaneous rotation of their spin and flavour in external magnetic fields (spin-flavour precession) [5, 6]. This precession can be resonantly enhanced in matter [7, 8]. The resonance spin-flavour precession of neutrinos (RSFP) in the matter and magnetic field of the sun can efficiently transform solar ν_{eL} into, e.g., $\nu_{\mu R}$ (or $\bar{\nu}_{\mu R}$ in the case of the transition magnetic moment of Majorana neutrinos) provided that the neutrino magnetic moment $\mu_\nu \gtrsim 10^{-11}\mu_B$ and the average strength of the solar magnetic field in the region where the transition takes place $B \gtrsim 40$ kG. As $\nu_{\mu R}$ or $\bar{\nu}_{\mu R}$ either do not interact with the detectors or interact with them more weakly than ν_{eL}, RSFP can account for the deficiency of observed solar neutrino flux. Analyses performed in the framework of this scenario [9, 10, 11, 12, 13] show that a very good fit of the currently available data can be achieved. In particular, the fits of the total detection rates are much better than those in the case of the Mikheyev-Smirnov-Wolfenstein (MSW [14]) effect whereas the fits of the recoil electron spectrum in Super-Kamiokande in the frameworks of the RSFP and MSW effect are of nearly the same quality [12, 13].

In the present paper we calculate, within the RSFP mechanism, the expected values of a number of observables to be measured by SNO. For three model solar magnetic field profiles that produce the best fits of the previous data we calculate the charged current event rate, the (neutral current)/(charged current) event ratio and the charged current electron spectrum as well as its first and second moments. We study the dependence of the calculated observables on the choice of the magnetic field profile and on the value of the solar *hep* neutrino flux. We then compare our results with those obtained by BKS assuming that the solar neutrino problem is due to neutrino oscillations in vacuum or in matter.

The implications of the RSFP of solar neutrinos for the SNO experiment have been analysed in the past [15, 16]. Our analysis is more detailed, especially as far as the charged current electron spectrum is concerned; in addition, we use the magnetic field profiles which

provide a good fit of all existing solar neutrino data, including the recent Super-Kamiokande ones which were not available when the analyses of [15, 16] were performed.

The paper is organized as follows: in sec. 2 we present the three magnetic field profiles to be used, in sec. 3 we define and evaluate the physical quantities which are relevant for the SNO experiment, for both the charged current (CC) and neutral current (NC) νd reactions. Finally in section 4 we discuss the obtained results and draw our main conclusions.

2 Solar magnetic field profiles

Unfortunately, very little is known about the inner magnetic field of the sun, and one is forced to use various model magnetic filed profiles in order to account for the solar neutrino data in the framework of the RSFP mechanism. In a previous paper [13] we investigated seven different magnetic field profiles and found that only some of them produce acceptable fits of the data. Here we present the three profiles which produced the best fits and which will be used in the present study. They are shown in figs. 1 and 2 of ref. [13] (notice that our present profiles 1, 2 and 3 are respectively profiles 2, 5 and 6 of ref. [13]).

All three profiles show a sudden rise around the bottom of the convective zone, at 0.65-0.71 of the solar radius followed by a smoother decrease up to the surface. Here the field intensity is at most of the order of a few hundred Gauss. The best fits quoted here were taken from ref. [13] and correspond to a neutrino magnetic moment $\mu_\nu = 10^{-11}\mu_B$ [1]. The first profile (profile 1) is [9]

$$B = 0\,, \qquad x < x_R. \tag{1}$$

$$B = B_0 \frac{x - x_R}{x_C - x_R}\,,\ x_R \le x \le x_C \tag{2}$$

$$B = B_0 \left[1 - \frac{x - x_C}{1 - x_C}\right]\,,\ x_C < x \le 1. \tag{3}$$

Here $x = r/R_\odot$, $R_\odot$ being the solar radius, and we take $x_R = 0.65$, $x_C = 0.80$. The best fit for the Homestake, SAGE, GALLEX, Kamiokande and Super-Kamiokande rates in this case corresponds to the values of the mass squared difference and peak field strength, respectively, $\Delta m^2_{21} = 1.20 \times 10^{-8}$ eV^2 and $B_0 = 1.23 \times 10^5$ G ($\chi^2/d.o.f. = 0.10/1$).

The next profile (profile 2) [17, 9] is

$$B = 0\,, \qquad x < x_R \tag{4}$$

$$B = \frac{B_0}{\cosh 30(x - x_R)}\,,\ x \ge x_R \tag{5}$$

with the best fit at $\Delta m^2_{21} = 2.1 \times 10^{-8}$ eV^2, $B_0 = 1.45 \times 10^5$ G ($\chi^2/d.o.f. = 0.055/1$).

[1] We recall that only the product of the magnetic moment and the magnetic field enters in the neutrino evolution equation and so our results apply to any other value of μ_ν provided that the magnetic field is rescaled accordingly.

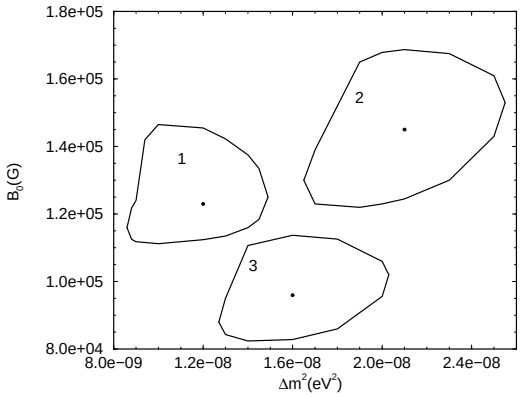

Figure 1: Regions in the (Δm^2_{21}, B_0) plane allowed at 90% c.l. by the combined fit of the Homestake, SAGE, Gallex, Kamiokande and Super-Kamiokande detection rates for the three magnetic field profiles used in the present study. Dots correspond to best fits.

Profile 3 [18] is a modification of the previous one:

$$B = 2.16 \times 10^3 \text{ G}\,, \qquad x \leq 0.7105 \tag{6}$$

$$B = B_1 \left[1 - \left(\frac{x - 0.75}{0.04}\right)^2\right]\,,\ 0.7105 < x < 0.7483 \tag{7}$$

$$B = \frac{B_0}{\cosh 30(x - 0.7483)}\,,\ 0.7483 \leq x \leq 1 \tag{8}$$

with $B_0 = 0.998 B_1$. The best fit is in this case is $\Delta m^2_{21} = 1.6 \times 10^{-8}$ eV^2, $B_0 = 9.6 \times 10^4$ G with $\chi^2/d.o.f. = 0.048/1$ [13]. The best fits of the Super-Kamiokande recoil electron spectrum found for these three profiles, at values of Δm^2_{21} and magnetic field strength rather close to those indicated above, were respectively $\chi^2 = 23.9, 23.5, 23.6$ for 16 d.o.f. [13]. In what follows we will be using the rate best fits.

We have determined the areas on the plane Δm^2_{21}, B_0 corresponding to the 90% c.l. fits of the data ($\chi^2 = \chi^2_{min} + 2.7$ for 1 d.o.f.) for each of the three magnetic field profiles described above. The resulting areas are shown in fig. 1 together with the best fit values.

3 Charged and neutral currents at SNO

SNO can detect solar neutrinos through the CC reaction

$$\nu_e + d \rightarrow p + p + e^- \tag{9}$$

(energy threshold $Q = 1.44$ MeV), NC reaction

$$\nu_x + d \rightarrow n + p + \nu_x \tag{10}$$

(energy threshold equal to the deuteron binding energy $E_B = 2.225$ MeV, $x = e\,,\ \mu$ or τ), and through the neutrino electron scattering $\nu_x + e \to \nu_x + e$. The rate and the recoil electron energy spectrum in the latter process at SNO are expected to be very similar to those at Super-Kamiokande studied in [13]; for this reason we shall not discuss them here.

We first consider the relative electron spectrum of reaction (9) which is defined as the ratio of the electron energy distribution and the corresponding distribution for standard model neutrinos. By standard model neutrinos we mean neutrinos described by the standard electroweak model (i.e. with no magnetic moment or mass) with their fluxes given by the standard solar model. We subdivide the electron energy spectrum into 0.5 MeV bins, with the relative spectrum for the i*th* bin given by

$$S_i = \frac{\int_{T_i}^{T_{i+1}} dT \int_Q^\infty dE\, f(E) P(E) \int_0^{E-Q} dT' \frac{d\sigma_{CC}}{dT'}(E,T') R(T,T')}{\int_{T_i}^{T_{i+1}} dT \int_Q^\infty dE f(E) \int_0^{E-Q} dT' \frac{d\sigma_{CC}}{dT'}(E,T') R(T,T')} \equiv \frac{\int_{T_i}^{T_{i+1}} dT\, dR_{CC}/dT}{\int_{T_i}^{T_{i+1}} dT\, dR^{st}_{CC}/dT} \quad (11)$$

Here $P(E)$ denotes the electron neutrino survival probability, T is the measured recoil electron kinetic energy, in contrast to the physical one, $T^{'}$. Following [20, 4], we approximate the energy resolution function of the detector $R(T', T)$ by a Gaussian

$$R(T,T') = \frac{1}{\Delta_{T'}\sqrt{2\pi}} \exp\left[-\frac{(T'-T)^2}{2\Delta^2_{T'}}\right], \qquad \Delta_{T'} = (1.1\text{ MeV})\sqrt{\frac{T'}{10\text{ MeV}}}\,. \quad (12)$$

The cross sections of the CC and NC νd reactions used throughout this paper are those of Kubodera *et al.* [22]. The SNO experiment is only sensitive to the high-energy ^{8}B and *hep* components of the solar neutrino flux. We use the BP98 solar neutrino spectrum $f(E)$ [19, 21] except that the *hep* neutrino flux is allowed to deviate from its nominal BP98 value. The *hep* flux is about 3 orders of magnitude smaller than that of ^{8}B neutrinos and so gives a negligible contribution to the CC and NC rates. However, its contribution to the highest energy part of the CC electron spectrum may be important as its endpoint energy is 18.8 MeV whereas that of ^{8}B neutrinos is only 15 MeV.

Unless otherwise specified, we consider the case of Majorana neutrinos in the present paper. The survival probability $P(E)$ is calculated by solving the RSFP evolution equation numerically [23]. The relative electron spectra for the three magnetic field profiles discussed in sec. 2 are shown in fig 2. The highest energy bin ($E_e \geq 14$ MeV) represents the average value of S for measured electron energies between 14 and 20 MeV. The solid lines correspond to the best fits whereas the dashed and dotted lines show the maximum and minimum values obtained within the 90% c.l. allowed regions of values of Δm^2_{21} and B_0 obtained by fitting the previous data and shown in fig. 1. In order to check the sensitivity of the spectrum to the poorly known *hep* flux we perform all the calculations for three values of the flux scaling factor, $f_{hep} = 0$, 1 and 20, with $f_{hep} = 1$ corresponding to the nominal *hep* flux value in the BP98 standard solar model (SSM).

We also calculate the first and second moments $\langle T \rangle$ and σ of the electron spectrum,

Table I: First moment $\langle T\rangle$ of the electron spectrum in the CC reaction (9) (in MeV) for three different magnetic field profiles and for standard model neutrinos. The results are presented for two values of the electron threshold energy $E_e = 5$ MeV and $E_e = 8$ MeV and two values of the *hep* neutrino flux scaling factor, $f_{hep} = 1$ and $f_{hep} = 20$ (indicated in the parentheses in the first line). The errors correspond to 90% c.l. (see the text for details).

Profile	$\langle T\rangle$ (5 MeV; 1)	$\langle T\rangle$ (8 MeV; 1)	$\langle T\rangle$ (5 MeV; 20)	$\langle T\rangle$ (8 MeV; 20)
1	$7.477 \pm {}^{0.124}_{0.126}$	9.117 ± 0.150	$7.541 \pm {}^{0.126}_{0.127}$	$9.198 \pm {}^{0.151}_{0.152}$
2	7.491 ± 0.125	9.121 ± 0.150	7.556 ± 0.126	9.202 ± 0.152
3	7.484 ± 0.125	9.119 ± 0.150	7.549 ± 0.126	9.200 ± 0.152
Stand. ν's	7.423 ± 0.122	9.101 ± 0.150	7.484 ± 0.123	9.179 ± 0.151

Table II: Same as in table I but for the second moment of the electron spectrum σ.

Profile	σ (5 MeV; 1)	σ (8 MeV; 1)	σ (5 MeV; 20)	σ (8 MeV; 20)
1	1.880 ± 0.070	1.273 ± 0.047	$1.953 \pm {}^{0.072}_{0.073}$	$1.385 \pm {}^{0.051}_{0.052}$
2	1.881 ± 0.070	1.274 ± 0.047	1.955 ± 0.072	1.387 ± 0.051
3	1.881 ± 0.070	1.273 ± 0.047	1.954 ± 0.072	1.386 ± 0.051
Stand. ν's	1.874 ± 0.069	1.267 ± 0.047	1.943 ± 0.072	1.375 ± 0.051

defined through

$$\langle T^n\rangle = \frac{1}{R_{CC}} \int_{T_m}^{\infty} T^n \, \frac{dR_{CC}}{dT}\, dT\,, \qquad R_{CC} = \int_{T_m}^{\infty} \frac{dR_{CC}}{dT}\, dT\,, \qquad \sigma = \sqrt{\langle T^2\rangle - \langle T\rangle^2}\,, \quad (13)$$

with dR_{CC}/dT defined in (11). The deviations of these moments from their values predicted by the SSM are convenient quantitative characteristics of the electron spectrum distortion [24]. The results of the calculations for two different values of the threshold electron kinetic energies T_m which correspond to the total energies of 5 MeV and 8 MeV and for $f_{hep} = 1$ and 20 are presented in tables I and II. We have also calculated $\langle T\rangle$ and σ for $f_{hep} = 0$ and found that their values are practically indistinguishable from those for $f_{hep} = 1$. This also applies to the CC event ratio r_{CC} and NC/CC double ratio $\bar{r}_{NC}$ discussed below. The errors presented in tables I and II include the 90% c.l. errors coming from the fits of the parameters Δm^2_{21} and B_0 (fig. 1) as well as from the uncertainties in the energy resolution and scale, ^{8}B neutrino spectrum, reaction cross section and statistics (assuming 5000 CC events). These uncertainties were taken from table II of ref. [4].

Next we examine the ratio of the CC event rate for neutrinos undergoing RSFP and that for standard model neutrinos,

$$r_{CC} = \frac{\int_{T_m}^{\infty} (dR_{CC}/dT)\, dT}{\int_{T_m}^{\infty} (dR^{st}_{CC}/dT)\, dT} = \frac{R_{CC}}{R^{st}_{CC}}\,. \quad (14)$$

This ratio depends on the chosen threshold energy T_m and we again use the same values of T_m

Table III: Ratio r_{CC} of the event rate due to the CC reaction (9) for neutrinos undergoing RSFP and that for standard model neutrinos. The values of the electron threshold energy and of the *hep* neutrino flux scaling factor f_{hep} are indicated in the parentheses in the first line. The errors correspond to 90% c.l. (see the text for details). The errors in the parentheses do not include the ^{8}B neutrino flux uncertainties.

Profile	r_{CC} (5 MeV; 1)	r_{CC} (8 MeV; 1)	r_{CC} (5 MeV; 20)	r_{CC} (8 MeV; 20)
1	$0.421\pm^{0.165(0.108)}_{0.121(0.050)}$	$0.431\pm^{0.169(0.111)}_{0.124(0.051)}$	$0.432\pm^{0.166(0.105)}_{0.124(0.049)}$	$0.450\pm^{0.177(0.110)}_{0.143(0.051)}$
2	$0.406\pm^{0.136(0.064)}_{0.116(0.046)}$	$0.415\pm^{0.139(0.066)}_{0.119(0.047)}$	$0.419\pm^{0.139(0.063)}_{0.119(0.046)}$	$0.436\pm^{0.145(0.066)}_{0.124(0.049)}$
3	$0.415\pm^{0.139(0.064)}_{0.119(0.048)}$	$0.426\pm^{0.142(0.066)}_{0.123(0.050)}$	$0.428\pm^{0.142(0.064)}_{0.122(0.048)}$	$0.446\pm^{0.148(0.067)}_{0.128(0.050)}$

that we used in calculating the moments of the electron spectrum. The results are presented in table III. The absolute values of the CC event rates for standard model neutrinos for the total electron threshold energies $E_e = 5$ MeV are 5.132 SNU and 5.253 SNU for $f_{hep} = 1$ and 20 respectively, and those for the electron threshold energy $E_e = 8$ MeV are 2.355 SNU and 2.451 SNU.

We have also calculated the total event rate of the NC reaction (10)

$$R_{NC} = \int_{E_B}^{\infty} f(E)\{P(E)\,\sigma_{NC}^{\nu d}(E) + [1 - P(E)]\,\sigma_{NC}^{\bar{\nu} d}(E)\}\epsilon(E)\,dE \tag{15}$$

Here $\epsilon(E)$ is the NC detection efficiency; following refs. [20, 4] we have taken $\epsilon(E) = 0.50$. For neutrino energies $E \leq 15$ MeV the cross sections of the NC νd and $\bar{\nu} d$ reactions differ by less than 7.3%, the difference at $E = 9$ MeV being about 4% [22]. These differences are within the uncertainty of the value of the NC cross sections itself, and to a good approximation one can put $\sigma_{NC}^{\bar{\nu} d}(E) = \sigma_{NC}^{\nu d}(E)$. The NC rate (15) then does not depend on the ν_e survival neutrino probability $P(E)$, and one therefore expects R_{NC} in the case of neutrinos undergoing RSFP to coincide with that for standard neutrinos R_{NC}^{st} [25, 16]. Notice that for $\mu_\nu \lesssim 10^{-11}\mu_B$ the electromagnetic contribution to the NC neutrino-deuteron disintegration reaction (10) due to the neutrino magnetic moment is more than eight orders of magnitude smaller than the standard electroweak one [26] and so can be safely neglected. For $f_{hep} = 1$ and 20 we obtain $R_{NC}^{st} = 1.216$ SNU and 1.242 SNU respectively.

An important characteristics of the νd reactions at SNO is the ratio $\bar{r}_{NC}$ of the ratios of the NC and CC event rates to their respective values for standard neutrinos. This double ratio is free of many uncertainties which are present in the single ratios r_{CC} and $r_{NC} \equiv R_{NC}/R_{NC}^{st}$. In particular, the errors in r_{CC} and r_{NC} due to the uncertainties in the flux of ^{8}B neutrinos practically cancel out in the double ratio, and those due to the uncertainties in the CC and NC cross sections cancel out to a large extent. As was mentioned above, for Majorana neutrinos one has $r_{NC} = 1$ to a good accuracy, and so $\bar{r}_{NC} = 1/r_{CC}$. The values of $\bar{r}_{NC}$ for the three magnetic field profiles that we consider are given in table IV. The indicated errors are the combined 90% c.l. ones coming from the uncertainties in

Table IV: Double ratio $\bar{r}_{NC} = r_{NC}/r_{CC}$. The values of the electron threshold energy for the CC reaction and of the *hep* neutrino flux scaling factor f_{hep} are indicated in the parentheses in the first line. The errors correspond to 90% c.l. (see the text for details).

Profile	$\bar{r}_{NC}$ (5 MeV; 1)	$\bar{r}_{NC}$ (8 MeV; 1)	$\bar{r}_{NC}$ (5 MeV; 20)	$\bar{r}_{NC}$ (8 MeV; 20)
1	$2.375\pm^{0.204}_{0.576}$	$2.320\pm^{0.200}_{0.566}$	$2.315\pm^{0.184}_{0.533}$	$2.222\pm^{0.177}_{0.511}$
2	$2.463\pm^{0.198}_{0.331}$	$2.410\pm^{0.187}_{0.329}$	$2.387\pm^{0.174}_{0.303}$	$2.294\pm^{0.165}_{0.296}$
3	$2.410\pm^{0.199}_{0.320}$	$2.347\pm^{0.196}_{0.308}$	$2.336\pm^{0.180}_{0.296}$	$2.242\pm^{0.173}_{0.284}$

the fitted values of Δm^2_{21} and B_0 (see fig. 1) as well as from the uncertainties in the electron energy resolution and scale in the CC reaction, ^{8}B neutrino spectrum, CC and NC cross sections and statistics (assuming 5000 CC events). The latter uncertainties were taken from table II of ref. [4].

Finally, we remark on the case of Dirac neutrino transition moments. In a sense this case is similar to neutrino oscillations into sterile neutrinos because the RSFP due to Dirac neutrino magnetic moments transforms ν_{eL} into sterile $\nu_{\mu R}$ or $\nu_{\tau R}$. The CC rate ratio r_{CC} in this case is similar to that in the Majorana neutrino case since the survival probabilities in the two cases are very close to each other. However, the NC rate R_{NC} and the rate ratio r_{NC} (and so the double ratios $\bar{r}_{NC}$) in the Majorana and Dirac cases are drastically different: while for Majorana neutrinos $R_{NC} \simeq R^{st}_{NC}$ ($r_{NC} \simeq 1$), in the case of Dirac neutrinos R_{NC} exhibits a suppression similar to that of R_{CC} and so the double ratio $\bar{r}_{NC}$ is close to unity. Thus, the double ratio $\bar{r}_{NC}$ can be used to discriminate between Dirac and Majorana neutrinos. We would like to stress that this is one of a very few known quantities that hold such a potential, the best known other example being the neutrinoless double beta decay. Notice that in general the RSFP of Dirac neutrinos leads to a fit of the solar neutrino data that is worse than that due to the RSFP of Majorana neutrinos and therefore we do not pursue here this possibility in detail.

4 Summary and discussion

We have investigated the expectations from the RSFP solution to the solar neutrino problem for the SNO experiment using the solar magnetic field profiles that provide the best fits for the rates of the Homestake, SAGE, GALLEX, Kamiokande and Super-Kamiokande experiments. We considered Majorana neutrinos and discussed the quantities that are relevant for the CC and NC processes (9) and (10) in SNO. To this end we have examined the expected relative CC electron spectrum $S(E_e)$ as well as the first and second moments of the spectrum $\langle T \rangle$ and σ, the ratio r_{CC} of the CC event rate to that of standard model neutrinos, and the ratio $\bar{r}_{NC}$ of the ratios of the NC and CC event rates to their respective values for standard neutrinos.

The values of the CC event rate ratio r_{CC} calculated for the electron threshold energies 5 MeV and 8 MeV are very close to each other, the difference being only 2 – 4% (table III). This is related to the the fact that, for the magnetic field profiles that we consider, the high-energy part of the survival probability $P(E)$ for neutrinos undergoing the RSFP is rather flat (see figs. 3 and 4 in [13]). Therefore both R_{CC} and R^{st}_{CC} decrease with increasing electron energy threshold to nearly the same extent so that their ratio r_{CC} changes very little. For the same reason the double ratio $\bar{r}_{NC}$, which depends on the CC electron threshold energy only through r_{CC}, is rather insensitive to the value of this threshold energy. In contrast to this, the first and second moments of the CC electron spectrum $\langle T \rangle$ and σ depend sensitively on the chosen electron threshold energy (see tables I and II).

To assess the sensitivity of the observables to be measured by SNO to the poorly known value of the *hep* neutrino flux we have performed all the calculations for three values of this flux: zero flux ($f_{hep} = 0$), the nominal flux of the BP98 standard solar model ($f_{hep} = 1$) and a factor of 20 larger one ($f_{hep} = 20$). Changing the value of f_{hep} from 0 to 1 does not lead to any noticeable difference in the calculated observables. The CC event rate ratio r_{CC} and the NC/CC double ratio $\bar{r}_{CC}$ only weakly depend on the value of the *hep* flux. This is mainly because the expected contributions of the *hep* neutrinos to the CC and NC event rates R_{CC} and R_{NC} are very small and even increasing these contributions by a factor of 20 would not change R_{CC} and R_{NC} much. The sensitivity to f_{hep} of the ratio r_{CC} and double ratio $\bar{r}_{NC}$ is further reduced due to a partial cancellation of the f_{hep} dependences of the numerators and denominators. The first moment of the CC electron spectra $\langle T \rangle$ is also rather insensitive to the *hep* neutrino flux: changing f_{hep} from 1 to 20 modifies $\langle T \rangle$ by less than 1%. The second moment σ is more sensitive to the *hep* neutrino flux: changing f_{hep} from 1 to 20 increases σ by about 4% for the electron energy threshold $E_{min} = 5$ MeV and by about 9% for $E_{min} = 8$ MeV. These features are independent of whether or not neutrinos undergo RSFP.

As can be seen from fig. 2, the high energy part of the relative CC electron spectrum ($E \gtrsim 12$ MeV) depends sensitively on the magnitude of the *hep* neutrino flux. For $f_{hep} = 20$ the excess of the number of the high energy events ($E \geq 14$ MeV) over the SSM prediction with nominal *hep* flux can be quite significant. It should be noted, however, that, although it is quite likely that the actual *hep* neutrino flux exceeds the nominal one of the BP98 model, the illustrative value $f_{hep} = 20$ that we used may in fact be too high. The most recent calculation [27] gives $f_{hep} \approx 5$.

All quantities that we have calculated have very similar values for the three magnetic field profiles that we chose. In particular, the values $\langle T \rangle$ and σ differ by less than 1% for different profiles, and those of r_{CC} and $\bar{r}_{NC}$ differ by 3 - 4%. This is the consequence of the fact that the magnetic field profiles used in our calculations, although rather different, lead to very similar ν_e survival probabilities $P(E)$ [13].

We shall now compare our predictions with those for standard neutrinos (with no magnetic moment or mass) and for neutrinos undergoing oscillations in vacuum or in matter. As can be seen from table III, the CC detection rates for neutrinos undergoing RSFP constitute about 40% of those for the standard neutrinos and SSM fluxes. The errors in r_{CC} are

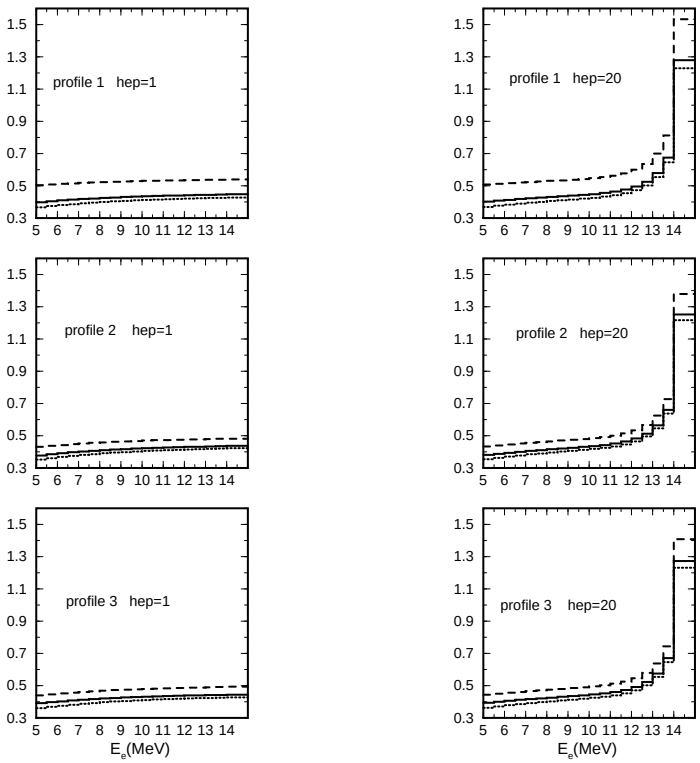

Figure 2: Relative CC electron spectra $S(E_e)$. Solid lines – best fits, dashed and dotted lines – maximum and minimum values corresponding to the allowed regions of fig. 1.

rather large (90% c.l. errors $\sim 35-40\%$), with about a half of their values coming from the uncertainty of the ^{8}B neutrino flux. The predicted values of r_{CC} differ from the SSM one $r_{CC}=1$ by about 5σ. However, for neutrinos of vanishing mass and magnetic moments, the ^{8}B neutrino flux measured by Super-Kamiokande, $\phi_{^8\mathrm{B}} = (0.475 \pm 0.015)\phi_{^8\mathrm{B}}^{\mathrm{SSM}}$, implies that the actual ^{8}B neutrino flux is about 0.48 of the one given by the SSM and so the expected value of the CC event rate ratio for standard neutrinos is $r_{CC} \simeq 0.48$ rather than $r_{CC}=1$. This value is less than 1σ away from our predictions given in table III, and so r_{CC} is not a suitable parameter for discriminating between standard and non-standard neutrinos.

The NC/CC double ratio $\bar{r}_{NC}$ has smaller errors (except for profile 1); it is practically independent of the uncertainty of the ^{8}B neutrino flux and in addition a number of other uncertainties of R_{CC} and R_{NC} drop out from this ratio. The calculated values of $\bar{r}_{NC}$ are of the order 2.5 and exceed the prediction for standard neutrinos $\bar{r}_{NC}=1$ by more than 7σ for profiles 2 and 3 and by about 4σ for profile 1. Thus $\bar{r}_{NC}$ is an ideal indicator of non-standard neutrinos.

The predicted relative CC electron spectrum $S(E_e)$ for $f_{hep}=1$ is rather flat (see fig. 2). For $f_{hep}=20$, one expects an excess of the high energy events. In both cases there is also a small decrease at low energies, $E \lesssim 8$ MeV. The shapes of the relative spectrum that we obtained for all three studied magnetic field profiles are very similar to each other and to that predicted for the SMA solution of the solar neutrino problem in the case of neutrino

oscillations (see fig. 3 in [4]). They are also similar to the $S(E_e)$ shape in the case of $\mathrm{VAC_S}$ oscillation solution, but the latter has a steeper increase at $E_e \gtrsim 10$ MeV. The shapes of the relative CC electron spectrum for LOW and LMA and $\mathrm{VAC_L}$ solutions differ from ours in that the former two are almost horizontal at low energies, whereas the latter one has a distinct dip in the energy range $E_e \simeq 8$ – 10 MeV.

Our predicted values of r_{CC} are typically slightly larger than those obtained in [4] for the LMA and LOW solution of the solar neutrino problem in the neutrino oscillation scenario, and in most part of the allowed range, also larger than those of the $\mathrm{VAC_S}$ solution studied by BKS (compare our table III with table V of [4]). Our values of r_{CC} are rather close to those for the SMA and $\mathrm{VAC_L}$ neutrino oscillation solutions. However, even in the case of the LMA and LOW solutions, there is a partial overlap with the RSFP predictions because the allowed regions of r_{CC} are rather large. The values of the NC/CC double ratio $\bar{r}_{NC}$ that we obtained are typically larger than those for the $\mathrm{VAC_L}$ solution, lower than those for the LMA and LOW solutions and similar to those for the SMA and $\mathrm{VAC_S}$ solutions studied in [4].

For an electron energy threshold of 5 MeV the best fit value of the first moment of the CC electron spectrum $\langle T \rangle$ in the case of the RSFP is systematically up-shifted compared to the SSM prediction by about (55 – 75) keV. The values of the shift $\langle \Delta T \rangle$ allowed at 90% c.l. range between -110 and $+230$ keV, which is about three times the expected combined calculational and measurement uncertainty, ± 96 keV [4]. For the electron threshold energy of 8 MeV the predicted range of $\langle \Delta T \rangle$ is somewhat larger, between -180 and $+215$ keV. Therefore in principle SNO holds a potential of measuring the shift in $\langle T \rangle$ due to non-standard neutrino properties. The shifts in $\langle T \rangle$ in the case of the RSFP have partial overlap with those predicted in the case of neutrino oscillations in vacuum or in matter [4]. Our predicted values of the shift in the second moment σ are smaller than those in $\langle T \rangle$. Their values allowed at 90% c.l. range between -70 and 82 keV, which has to be compared with the 1σ uncertainty of ± 44 keV. Again, there is a partial overlap between our predictions for $\Delta\sigma$ and those in the case of neutrino oscillations [4], but there are also rather large regions of no overlap, especially in the case of $\mathrm{VAC_S}$ and $\mathrm{VAC_L}$ oscillation solutions.

We therefore conclude that the possibility of experimentally disentangling the two types of solutions to the solar neutrino problem (neutrino oscillations and magnetic moments) depends to a large extent on where in the allowed region the neutrino parameters lie. Given the uncertainties in the calculations and the expected uncertainties in the experimental results, the unambiguous discrimination on the basis of the average rates and electron spectrum distortions appears to be difficult.

On the other hand, the RSFP mechanism can lead to time dependence of the solar neutrino signal due to the variability of the solar magnetic field strength. Such time dependence should be manifest in the CC reaction rate and electron spectrum, but should not be observable in the NC rate provided that neutrinos are Majorana particles [25, 16]. In particular, the CC signal can have an 11-year periodicity related to the solar activity cycle [23]. There may also be seasonal variations of the CC signal due to the surface equatorial

gap in the toroidal magnetic field of the sun and a non-zero angle between the solar equatorial plane and the earth's ecliptic [6]. These seasonal variations are expected to be different from those expected in the case of $\mathrm{VAC_S}$ and $\mathrm{VAC_L}$ oscillation solutions. However, the gap in the magnetic field seen at the surface of the sun may not be present in the inner regions where the RSFP effectively takes the place. It is therefore difficult to make an unambiguous prediction on whether or not the seasonal variations of the CC signal should take place in the case of the RSFP scenario.

If both transition magnetic moments and mixing of massive neutrinos are present, the combined action of the RSFP and neutrino oscillations may lead to an observable flux of solar $\bar{\nu}_e$'s [7, 28] provided that the mixing angle is not too small, $\sin 2\theta_0 \gtrsim 0.1$. SNO can detect $\bar{\nu}_e$ through the CC reaction $\bar{\nu}_e + d \to n + n + e^+$ (for a recent discussion of the $\bar{\nu}_e$ signal in SNO see the second reference in [9]).

Thus, the possible time dependence of the CC signal and spectrum distortion together with the time independence of the NC signal in the case of the magnetic moment solution remains the best hope for a discrimination between the neutrino magnetic moment and oscillation scenarios. For a hybrid solution (neutrino magnetic moment plus flavour mixing) the smoking gun signature would be an observation of $\bar{\nu}_e$'s from the sun.

We are grateful to K. Kubodera for useful correspondence. The work of E. A. was supported by Fundação para a Ciência e a Tecnologia through the grant PRAXIS XXI/BCC/16414/98 and also in part by the TMR network grant ERBFMRX-CT960090 of the European Union.

References

[1] A.B. McDonald, Nucl. Phys. Proc. Suppl. 77 (1999) 43; SNO Collaboration, J. Boger *et al.*, nucl-ex/9910016.

[2] Homestake Collaboration, B. T. Cleveland *et al.*, Astrophys. J. 496 (1998), 505; SAGE Collaboration, J. N. Abdurashitov *et al.*, astro-ph/9907113; Gallex Collaboration, P. Anselmann *et al.*, Phys. Lett. B 447 (1999) 127; Kamiokande Collaboration, Y. Fukuda *et al.*, Phys. Rev. Lett. 77 (1996) 1683; Super-Kamiokande Collaboration, Y. Fukuda *et al.*, Phys. Rev. Lett. 81 (1998) 1158 (Erratum - *ibid.* 81 (1998) 4279); *ibid.* 82 (1999) 1810; *ibid.* 82 (1999) 2430.

[3] J. N. Bahcall, P. I. Krastev and A. Yu. Smirnov, Phys. Lett. B477 (2000) 401.

[4] J. N. Bahcall, P. I. Krastev and A. Yu. Smirnov, hep-ph/0002293.

[5] J. Schechter and J. W. F. Valle, Phys. Rev. D 24 (1981) 1883; Erratum-*ibid.* D 25 (1982) 283.

[6] L.B. Okun, M.B. Voloshin, M.I. Vysotsky, Sov. Phys. JETP 64 (1986) 446; Erratum - *ibid.* 65 (1987) 209.

[7] C. S. Lim, W. J. Marciano, Phys. Rev. D 37 (1988) 1368.

[8] E. Kh. Akhmedov, Sov. J. Nucl. Phys. 48 (1988) 382; Phys. Lett. B 213 (1988) 64.

[9] E. Kh. Akhmedov, A. Lanza and S. T. Petcov, Phys. Lett. B 303 (1993) 85; *ibid.* B 348 (1995) 124.

[10] J. Pulido, Phys. Rev. D 48 (1993) 1492.

[11] C.S. Lim, H. Nunokawa, Astropart. Phys. 4 (1995) 63.

[12] M. Guzzo and H. Nunokawa, Astropart. Phys. 12 (1999) 87.

[13] J. Pulido, E.Kh. Akhmedov, Astropart. Phys. 13 (2000) 227.

[14] L. Wolfenstein, Phys. Rev. D 17 (1978) 2369; S. P. Mikheyev, A. Yu. Smirnov, Sov. J. Nucl. Phys. 42 (1985) 913.

[15] A.B. Balantekin, F. Loreti, Phys. Rev. D 45 (1992) 1059; *ibid.* D 48 (1993) 5496.

[16] S.M. Bilenky, C. Giunti, hep-ph/9312211; Astropart. Phys. 2 (1994) 353.

[17] E. Kh. Akhmedov and O.V. Bychuk, Sov. Phys. JETP 68 (1989) 250.

[18] J. Pulido, Phys. Rev. D 57 (1998) 7108.

[19] J. N. Bahcall, S. Basu and M. H. Pinsonneault, Phys. Lett. B 433 (1998) 1.

[20] J.N. Bahcall, E. Lisi, Phys. Rev D 54 (1996) 5417.

[21] J. N. Bahcall's homepage, http://www.sns.ias.edu/∼jnb/.

[22] Y. Kohyama, K. Kubodera, USC (NT) Report 92-1, 1992 (unpublished); K. Kubodera, S. Nozawa, Int. J. Mod. Phys. E 3 (1994) 101; K. Kubodera's homepage, http://nuc003.psc.sc.edu/∼kubodera/.

[23] For reviews, see, e.g., J. Pulido, Phys. Rep. 211 (1992) 167; E.Kh. Akhmedov, hep-ph/9705451.

[24] J.N. Bahcall, P.I. Krastev, E. Lisi, Phys. Rev. C55 (1997) 494; S.P. Mikheyev, A.Yu. Smirnov, Phys. Lett. B 429 (1998) 343.

[25] E.Kh. Akhmedov, preprint IAE-5017/1, 1990 ; Nucl. Phys. A527 (1991) 679c.

[26] E.Kh. Akhmedov, V.V. Berezin, Z. Phys. C54 (1992) 661.

[27] L.E. Marcucci *et al.*, nucl-th/0003065.

[28] E.Kh. Akhmedov, Sov. Phys. JETP 68 (1989) 690.